Supporting information

Ru/Mo_2C@NC Schottky Junction-loaded Hollow Nanosphere as Efficient Hydrogen Evolution Electrocatalyst

Abdulwahab Salah [a,d], Hong- Da Ren [a], Nabilah Al-Ansi [c,d], Fei-Yang Yu [a], Zhong-Ling Lang*[b], Huaqiao Tan*[a], and Yang-Guang Li *[a]

[a] *Key Laboratory of Polyoxometalate and Reticular Material Chemistry of Ministry of Education, Faculty of Chemistry Northeast Normal University, Changchun 130024, China. E-mail: tanhq870@nenu.edu.cn, liyg658@nenu.edu.cn*

[b] *Centre for Advanced Optoelectronic Functional Materials Research and Key Laboratory of UV-Emitting Materials and Technology, Ministry of Education, Northeast Normal University, Changchun 130024, China. E-mail: langzl554@nenu.edu.cn*

[c] *Faculty of Chemistry, National and Local United Engineering Laboratory for Power Batteries, Northeast Normal University, Changchun, 130024 P. R. China.*

[d] *Department of Science Curricula & Teaching Methodologies, Faculty of Education, Sana'a University, Yemen.*

Table of contents

1. Experimental section

1.1. Chemical reagents

Ammonium molybdate tetrahydrate ($(NH_4)_6Mo_7O_{24}\cdot 4H_2O$), dopamine hydrochloride ($C_8H_{11}NO_2\cdot HCl$), ruthenium chloride trihydrate ($RuCl_3\cdot 3H_2O$), and potassium hydroxide (KOH) were purchased from Aladdin Industrial Co., Ltd. Commercial 20 % Pt/C, 5 % Ru/C, Ru powder catalysts, and Nafion solution (5 wt. %) were purchased from Alfa Aesar China (Tianjin) Co., Ltd. Ammonium hydroxide (25–28 wt. %), anhydrous ethanol (EtOH), NaSCN, and XC-72 carbon were purchased from Macklin. All solvents and chemicals were used as bought without further purification. Millipore water (18.2 MΩ cm, 25 °C) was used to prepare all solutions used in our experiments.

1.2. Working electrodes preparation

The catalyst ink of each working electrode was prepared via dispersing 3 mg of the catalyst in 300 μL of the mixture of 0.5 wt. % Nafion and ethanol with a mass ratio of 1: 9, respectively. After ultrasonication for 30 min, the ink was ready. Then, 5 μL of the ready ink was being dropped onto the glassy carbon electrode (GCE, 3 mm) and dried in the air, resulting in the loading of an approximate 0.708 mg cm^{-2} of the catalyst.

2. Characterization techniques and other Supplements

2.1. Instruments characterization

The structures of samples were analyzed by using the scanning electron microscopy (SEM) on the Hitachi SU-8010 instrument at an accelerating voltage of 3 kV and transmission electron microscopy (TEM; JEOL-2100F). The powder X-ray diffraction

(XRD) patterns were collected on a Rigaku Smart Lab X-Ray diffractometer operated at 20 mA and 40 kV with Cu Ka radiation at room temperature (λ=1.5418 Å). Raman spectrum was conducted on a Raman spectrometer (JY, Labram HR 800). The element composition and valence states of samples were measured by X-ray photoelectron spectroscopy (XPS, KRATOS Axis ultra DLD X-ray photoelectron spectrometer, USA) using Mg Kα radiation (hυ = 1283.3 eV) as a source of excitation. The energy dispersive X-ray detector (EDX) measurements were carried out utilizing a SU8000 ESEM FEG microscope. The nitrogen adsorption-desorption measurement was realized on an ASAP 2020 (Micromeritics, USA). The inductively coupled plasma-atomic emission spectroscopy (ICP-AES) elemental analyses were achieved on a Prodigy Leeman ICP-AES spectrometer to quantify the Ru concentration in different catalysts. The evolved gases during HER were determined by gas chromatography (Shimadzu, GC-2014C) connecting the electrochemical workstation.

2.2. Electrochemical measurements

All electrochemical measurements were recorded using the three-electrode system at 25 °C and connected to a CHI760E electrochemical workstation (CH Instruments, China). a glassy carbon electrode (GCE; d = 0.3 cm), Ag/AgCl in saturated 3 M KCl solutions, and a graphite rod were used as working electrodes, a reference, and a counter, respectively. Linear sweep voltammetry (LSV), cyclic voltammetry (CV), electrochemical impedance spectroscopy (EIS), and amperometric (i-t) measurements were executed using a CHI760E workstation (CH Instruments, China). All the potentials were accomplished contra an Ag/AgCl electrode and transformed to a reversible hydrogen electrode (RHE) according to $E_{RHE} = E_{Ag/AgCl} + E^0_{Ag/AgCl} + 0.059 \times pH$. The HER polarization curves were corrected by

removing iR_s from the measured potential, according to the following equation: $E_{corrected} = E_{measured} - iR_s$. Where $E_{corrected}$, $E_{measured}$, and i are the iR-corrected potential, experimental potential measurement, and current, respectively. The LSV curves were replaced as overpotential (η) versus the logarithm of the current density (log |j|) to get the Tafel plots by fitting the linear portion of the Tafel plots, according to the Tafel equation ($\eta = b \log j + a$, where η, b, j, and a represent the overpotential, Tafel slope, current density, and the intercept relative to the exchange current density (j_0), respectively).[S1, 2] LSV data were recorded at a scan rate of 5 mV s^{-1} in different electrolytes. The electrochemical impedance spectroscopy (EIS) measurements were achieved during a frequency range from 0.01 to 100 kHz with an amplitude of 10 mV, and then the spectra of EIS were evaluated using the Z-SimpWin software. The electrochemical active surface areas (ECSA) of catalysts were earned from simple cyclic voltammetry (CV) curves that were carried out in the potential range with no faradic current at different scan rates from 25 to 200 mV s^{-1}. The ECSA was assessed by the double-layer capacitance (Cdl) proportional to it. The value of Cdl was estimated via plotting the Δj ($j_a - j_c$) in a certain potential versus the scan rate, and the slope is twice Cdl.[S3] The ECSA was designated using standard cyclic voltammetry (CV) sweeps at scan rates from 25 to 200 mV s^{-1} in the voltage region devoid of faradic current from -0.90 to -0.80 V (vs. Ag/AgCl) in 1 M KOH, from and -0.10 to 0.00 V (vs. Ag/AgCl) in 0.5 M H_2SO_4, and from -0.50 to -0.40 V (vs. Ag/AgCl) in 1 M PBS. The electrochemical cycling stability was experienced by using continuous CV sweeps for 5000 cycles at a scan rate of 0.1 V s^{-1} in the potential range from -1.30 to -1.0 V (vs. Ag/AgCl) in 1 M KOH, from -0.70 to 0.10 V (vs. Ag/AgCl) in 0.5 M H_2SO_4, and from -0.30 to 0.60 V (vs.

Ag/AgCl) in 1 M PBS. Also, the long-term stabilities at different electrolytes were investigated using amperometric (i-t) measurements under fixed overpotentials.

2.3. Hydrogen generation mechanism in the alkaline media

By benefiting from the mechanism of HER in catalysts based on Schottky junction formation between metal and semiconductor,[S4-6] the hydrogen generation steps by the electrocatalysis of the Ru/Mo_2C@NC Schottky junction in the alkaline media are as follows: (1) From the direct current power source, Mo_2C-semiconductor soaks up the energy required to separate electrogenerated carriers and electrons transition to the conduction band from the valence band. (2) Electrons that have reached the conduction band of Mo_2C-semiconductor move to Ru species via the Schottky junction. (3) The existing electrons on the Ru species interact with the H^+ in the alkaline solution to produce H_2 on the catalyst surface.

It is also known that the mechanism of hydrogen generation in the alkaline media usually includes three essential reactions, according to the following equations:[S7-10]

$$H_2O + M + e^- \rightleftharpoons MH_{ads} + OH^- \quad (1)\ \text{Volmer step} \quad (120\ \text{mV dec}^{-1})$$

$$H_2O + e^- + MH_{ads} \rightleftharpoons M + H_2 + OH^- \quad (2)\ \text{Heyrovsky step} \quad (40\ \text{mV dec}^{-1})$$

$$MH_{ads} + MH_{ads} \rightleftharpoons 2M + H_2 \quad (3)\ \text{Tafel step} \quad (30\ \text{mV dec}^{-1})$$

Where MH_{ads} denotes the hydrogen atoms adsorbed at the active sites in the catalysts (M). The first step includes the reaction of discharged with a Tafel slope value of 120 mV dec^{-1} (Volmer reaction), forming adsorbed hydrogen (H_{ads}). Next, the H_{ads} may comport one of the following reactions to generate H_2: the recombination step of H_{ads} on the catalyst

surface with a Tafel slope of 30 mV dec^{-1} (Tafel slope) or the electrochemical desorption step with a Tafel slope of 40 mV dec^{-1} (Heyrovsky reaction).

2.4. TOF calculations

Turnover frequency (TOF) is usually calculated through the following equation: $TOF = I/2nF$, where I, n, and F represent the current (A) in the LSV measurement in the electrolyte, number moles of active sites for the catalyst, and faraday constant (96500 C mol^{-1}), respectively.[S11] The factor *1/2* comes from the fact that one hydrogen molecule takes two electrons to produce two protons.

2.5. Determination of Faradaic efficiency

The faradaic efficiency of any catalyst in the HER process is known as the ratio of the number of H_2 equivalents produced experimentally to that expected based on theoretical calculations for the reaction. The experiments were achieved in the typical airtight H-type cell with a three-electrode system. Nafion 117 proton exchange membrane was used to separate cathode and anode compartments, and the electrolyte was bubbled with N_2 for 0.5 h before doing experiments. The gaseous product was analyzed by combined gas chromatography with an electrochemical workstation. The electrolytic cell was continuously saturated with N_2 at a steady flow rate of 100.00 sccm and injected directly into a gas chromatograph device's gas-sampling loop during the hydrogen production process. Regarding the theoretical value, it has been assumed that the current efficiency is 100 % during the reaction, where the HER process occurs only on the working electrode. Faraday law was used to calculate the theoretical amount of H_2 evolution, which states that the passage of 96485.4 C of charge causes 1 equivalent of reaction[S12].

3. Supporting Figures

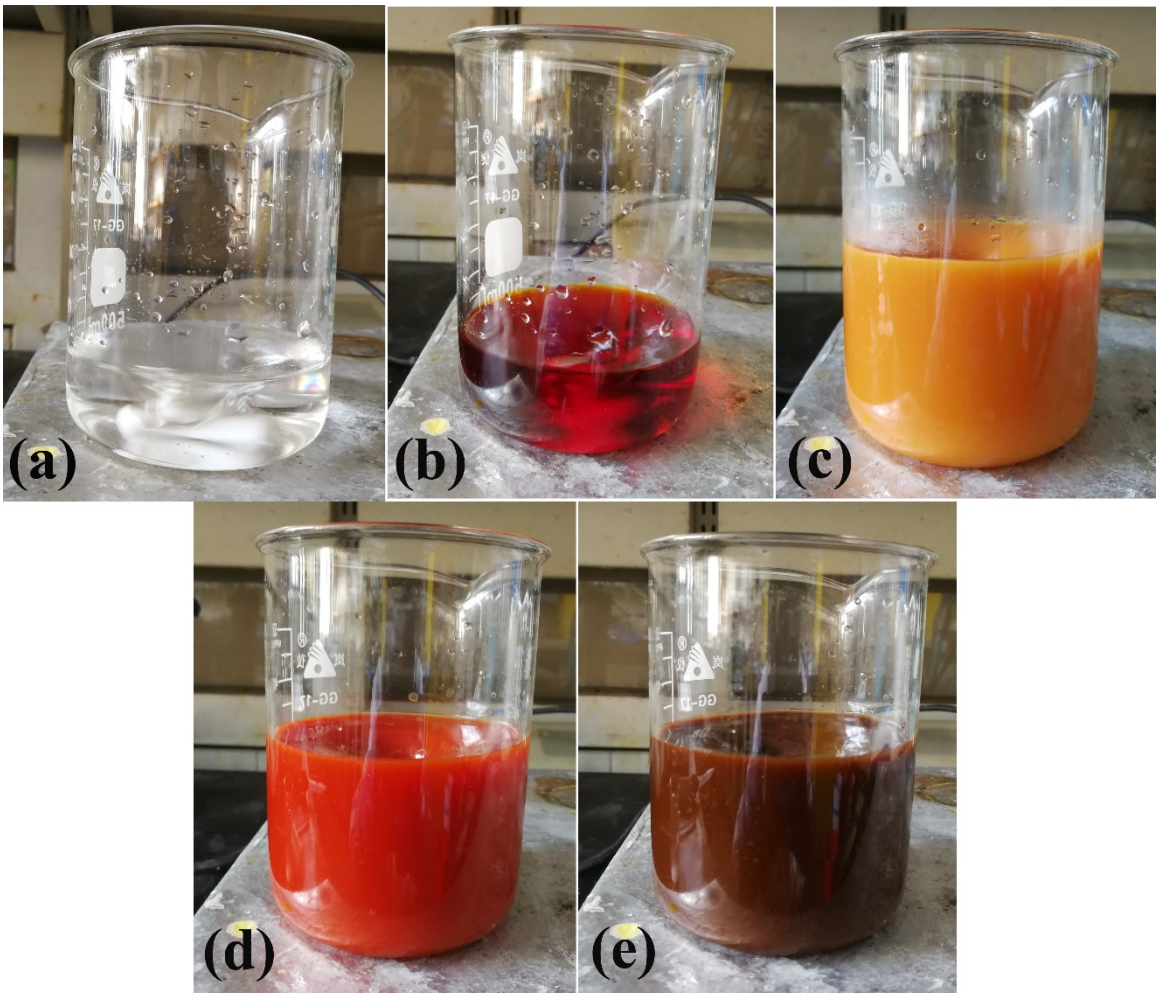

Fig. S1 Optical photograph of stirring synthesis of Ru/Mo-polydopamine hollow nanosphere (Mo-PDA HS) under room temperature 25 °C; (a) $(NH_4)_6Mo_7O_{24}\cdot 4H_2O$ with H_2O, (b) $(NH_4)_6Mo_7O_{24}\cdot 4H_2O$ with dopamine-HCl before added ethanol, (c) $(NH_4)_6Mo_7O_{24}\cdot 4H_2O$ with dopamine-HCl after added ethanol, (d) $(NH_4)_6Mo_7O_{24}\cdot 4H_2O$ with dopamine-HCl after added ethanol and after adjusting pH to (8.6-9) with 25 % NH_4OH (Mo-PDA HS), and (e) Mo-PDA HS after added $RuCl_3.3H_2O$.

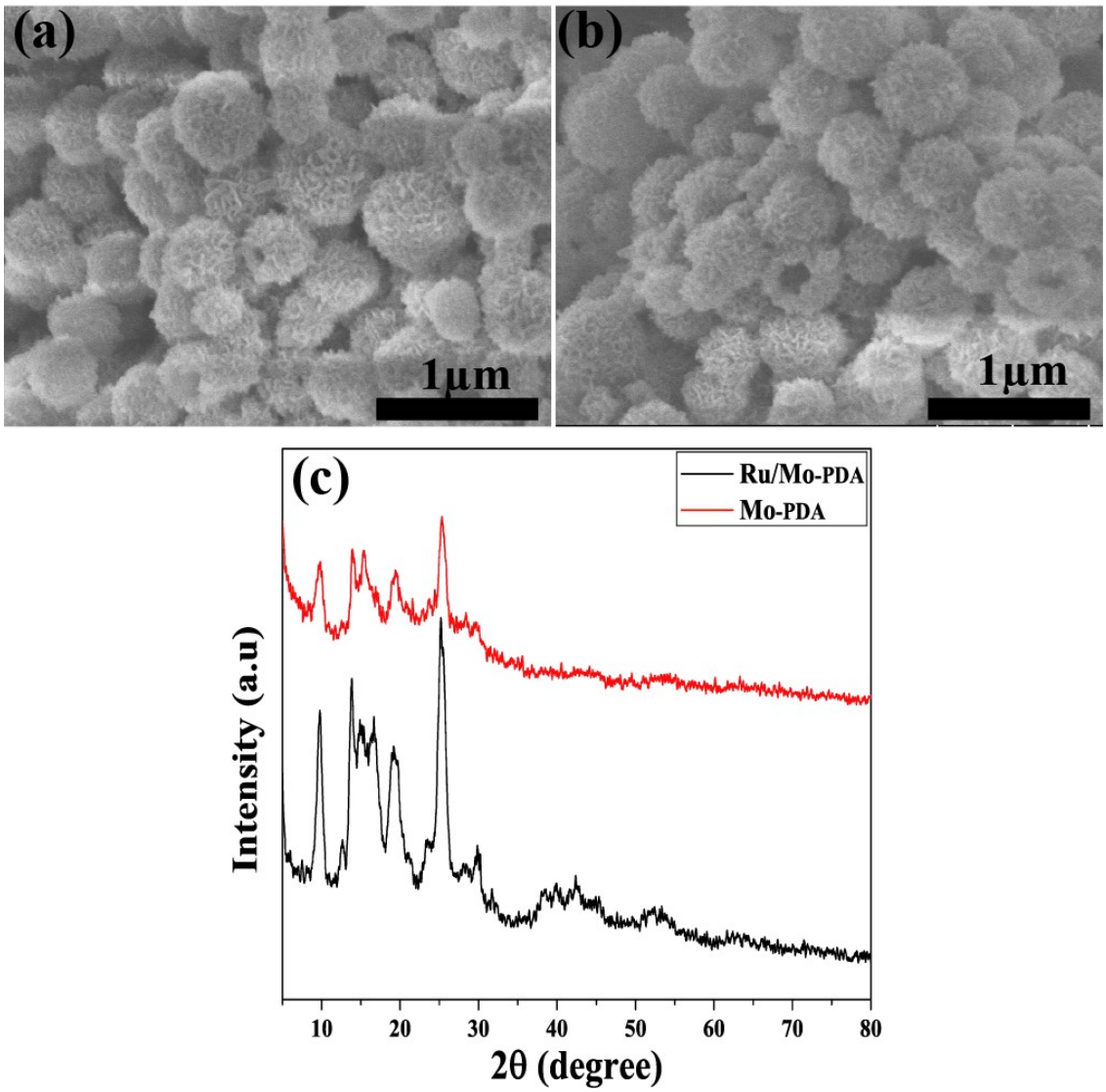

Fig. S2 (a) and (b) SEM images of Mo-PDA HS and Ru/Mo-PDA HS. (c) XRD patterns corresponding to these composites.

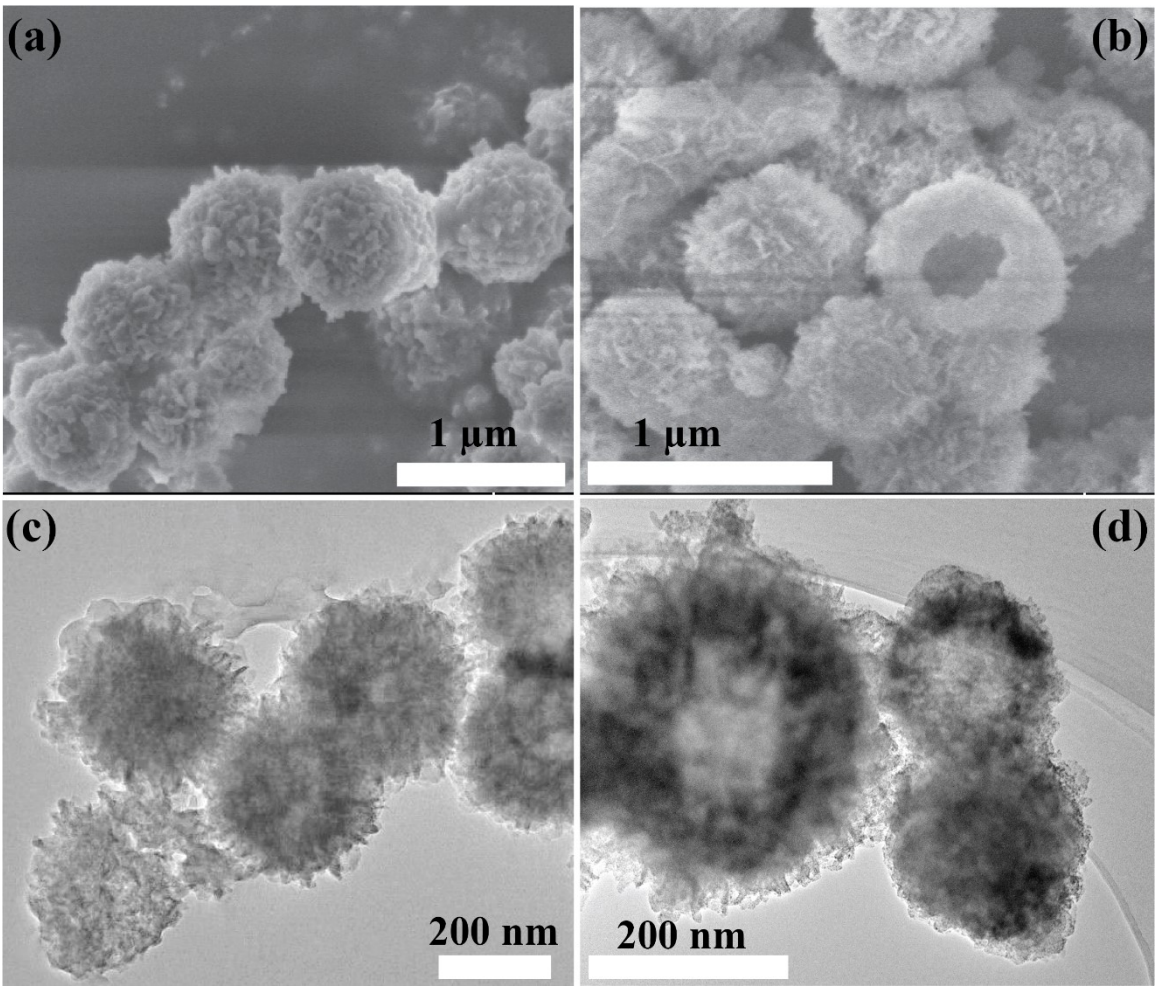

Fig. S3 SEM and TEM images of Mo-PDA with different volume ratios of water to ethanol (a,d) 1:1, and (b,e) 1:2.

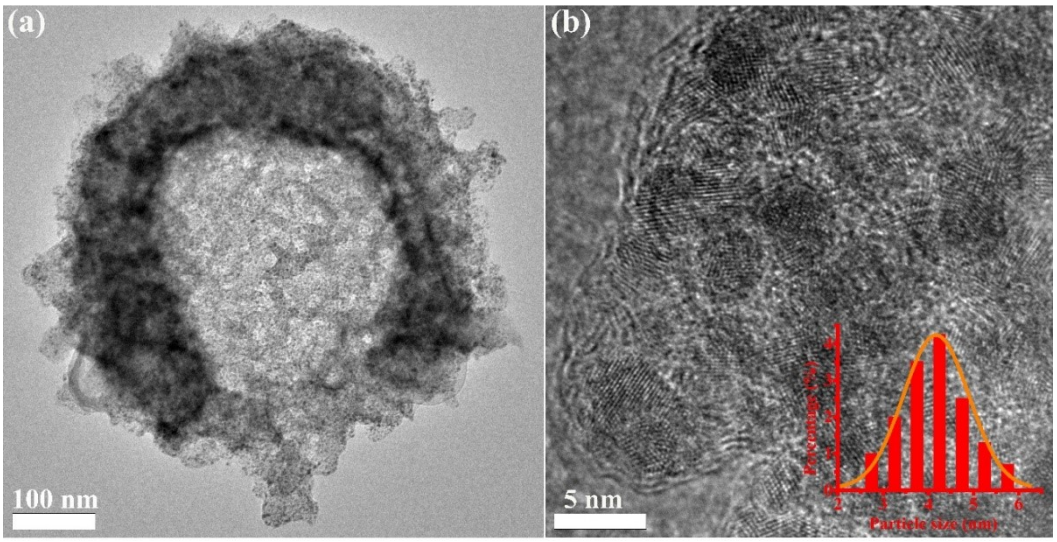

Fig. S4 (a) TEM, (b) HRTEM images of Ru/Mo_2C@NC (Ru wt. % = 3.93 %) catalyst; insets (b): Particle size distributions of Ru/Mo_2C Schottky junction.

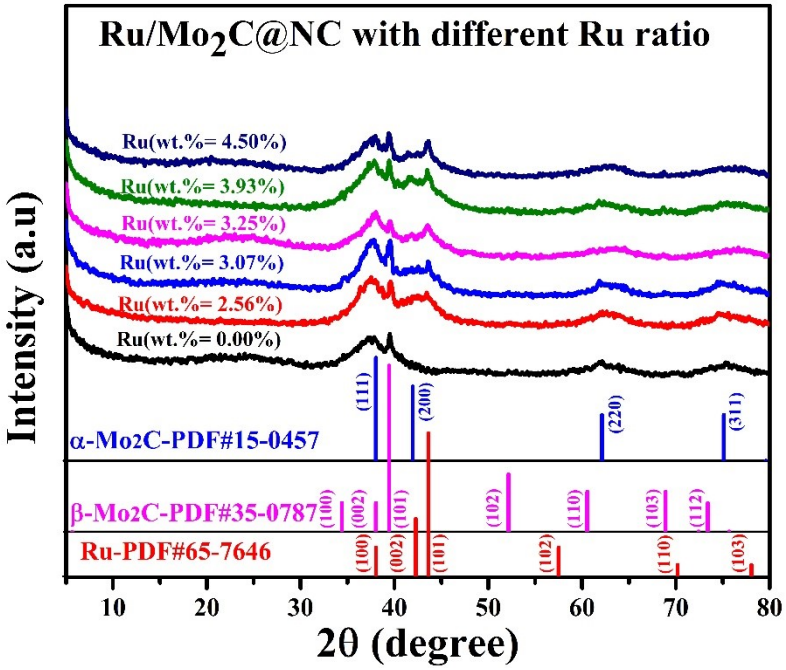

Fig. S5 XRD patterns of a series of Ru/Mo_2C@NC catalysts with different Ru mass loading (Ru wt. % = 0.00, 2.56, 3.07, 3.25, 3.93, and 4.50 %).

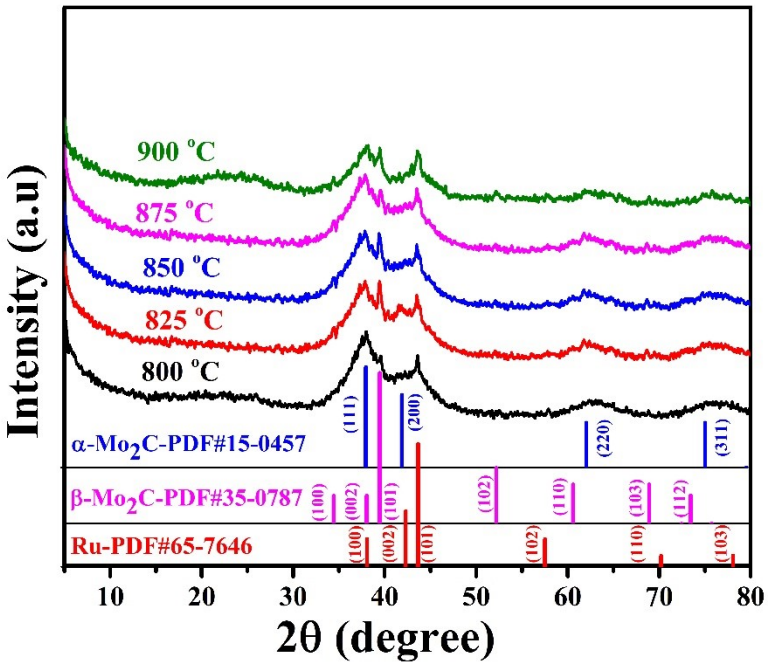

Fig. S6 XRD patterns of a series of Ru/Mo_2C@NC (Ru wt. % = 3.93 %) catalysts prepared at different temperatures in the range from 800 °C to 900 °C.

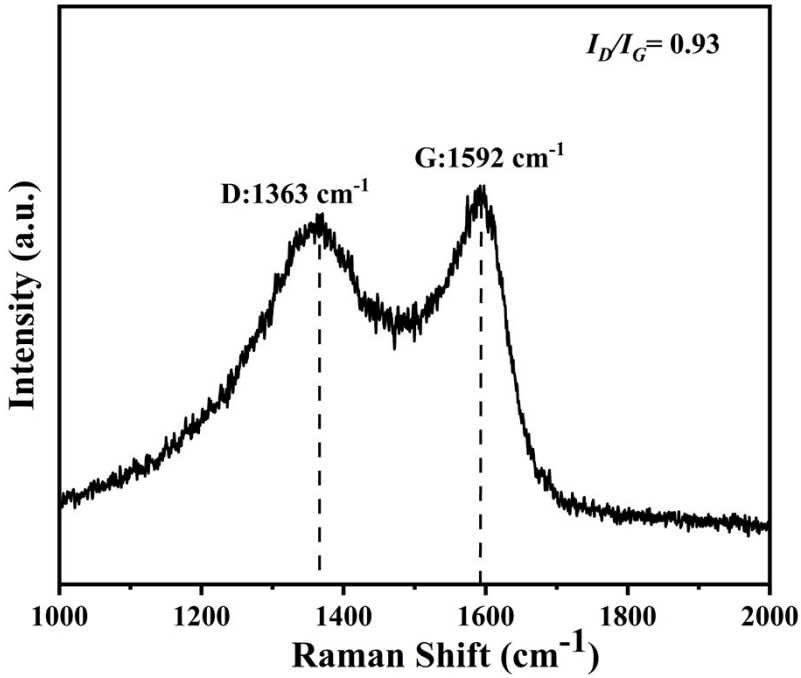

Fig. S7 Raman spectrum of Ru/Mo_2C@NC (Ru wt. % = 3.93 %) catalyst.

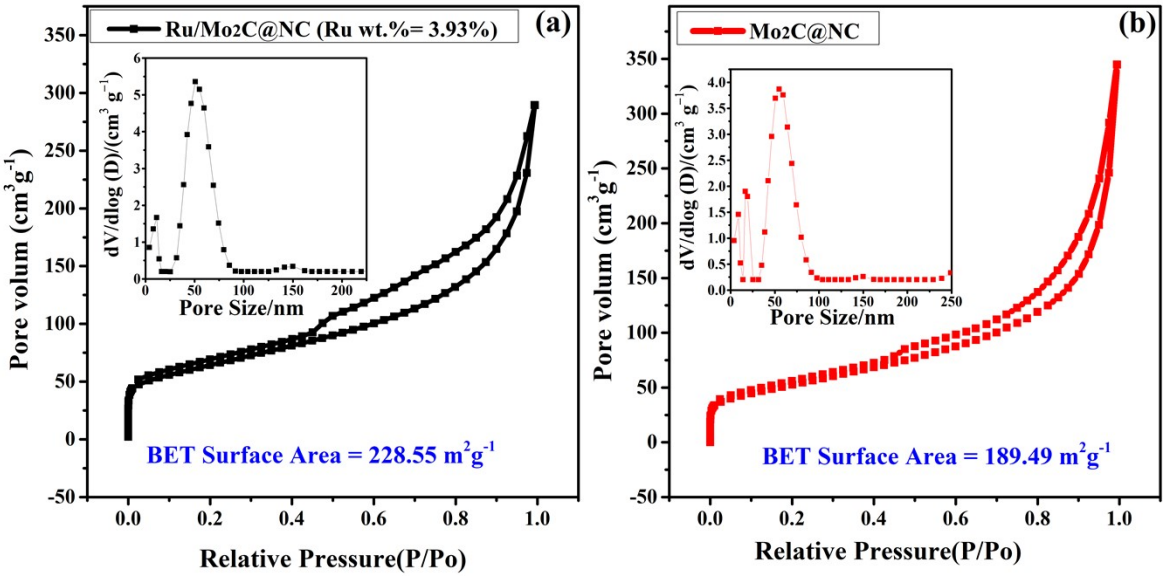

Fig. S8 (a) and (b) N_2 adsorption-desorption measurements at 77 K of Ru/Mo_2C@NC (Ru wt. % = 3.93 %) and Ni/WC@NPC catalysts. The insets of images are the corresponding pore size distributions of these catalysts.

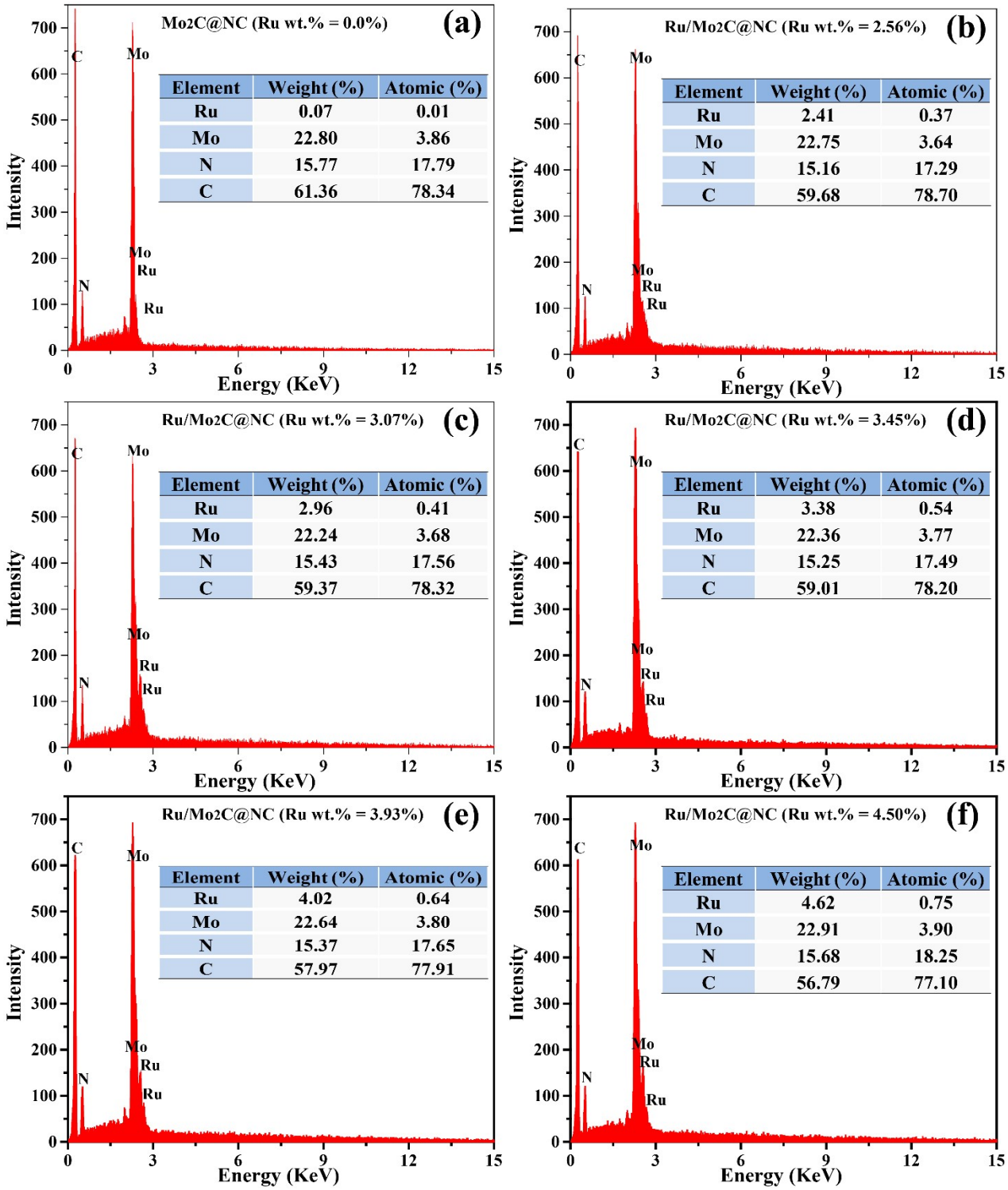

Fig. S9 (a-f) EDX spectra for a series of Ru/Mo_2C@NC catalysts with different mass loading of Ru element.

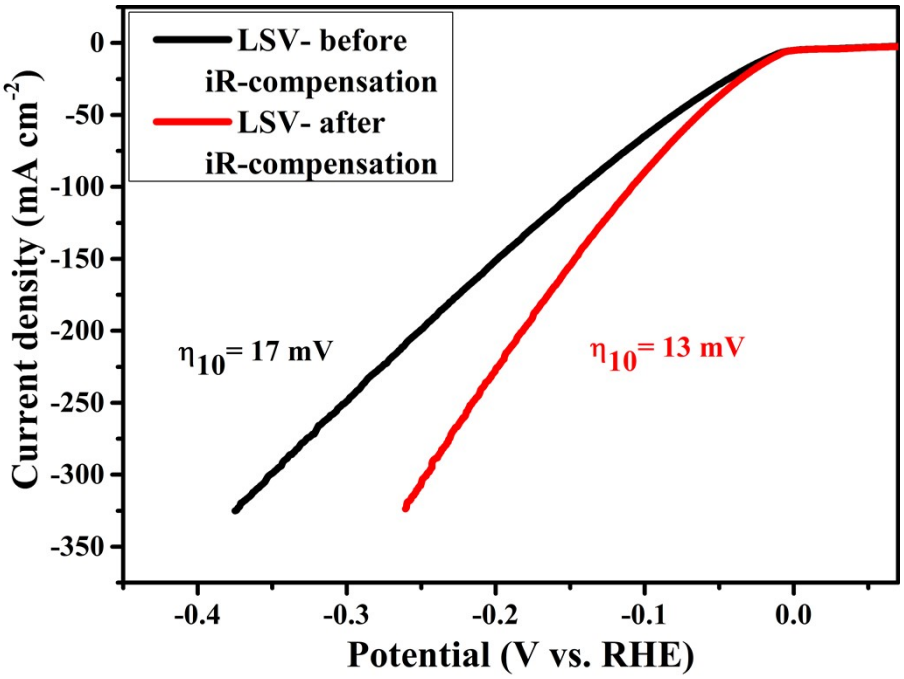

Fig. S10 LSV curves of Ru/Mo_2C@NC (Ru wt. % = 3.93 %) catalyst in 1 M KOH without and with *iR*-compensation at a scan rate of 5 mV s^{-1}.

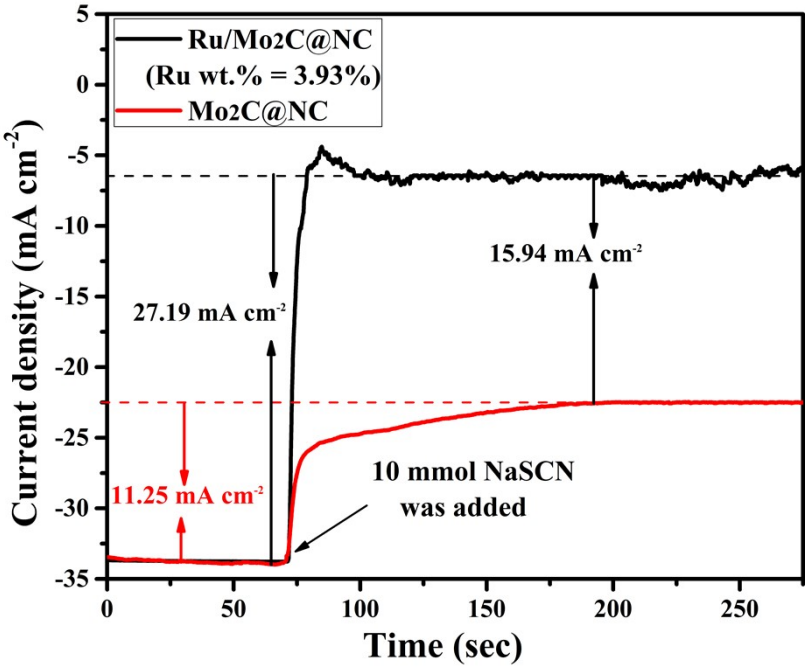

Fig. S11 i-t curves of Ru/Mo_2C@NC (Ru wt. % = 3.93 %) and Mo_2C@NC before and after adding 10 mmol of SCN^- ions in 1 M KOH.

As shown in the above i-t curves, the current densities for both Ru/Mo_2C@NC (Ru wt. % = 3.93 %) and Mo_2C@NC exhibit a clear decayed after adding 10 mmol of SCN^- at

t = 200 s. The current density of Ru/Mo_2C@NC (Ru wt. % = 3.93 %) reduces from 33.71 to 6.52 mA cm^{-2} (the decaying ratio of current density is 80.66 %), while the current density of Mo_2C@NC decreases from 33.71 to 22.46 mA cm^{-2} (the decaying ratio of current density is 33.37 %). This result strongly confirms that the Ru NPs act as the active sites in the Ru/Mo_2C@NC (Ru wt. % = 3.93 %) catalyst and booking by SCN^- ions.

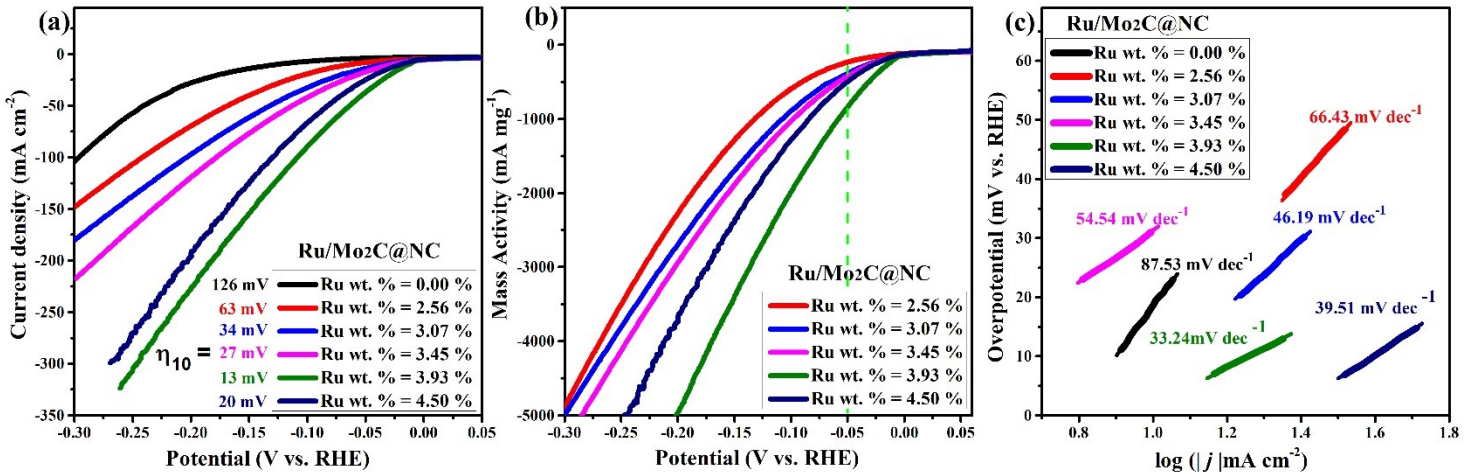

Fig. S12 (a) LSV curves, (c) mass activities, and (c) Tafel plots of Ru/Mo_2C@NC with different Ru mass ratios in 1 M KOH.

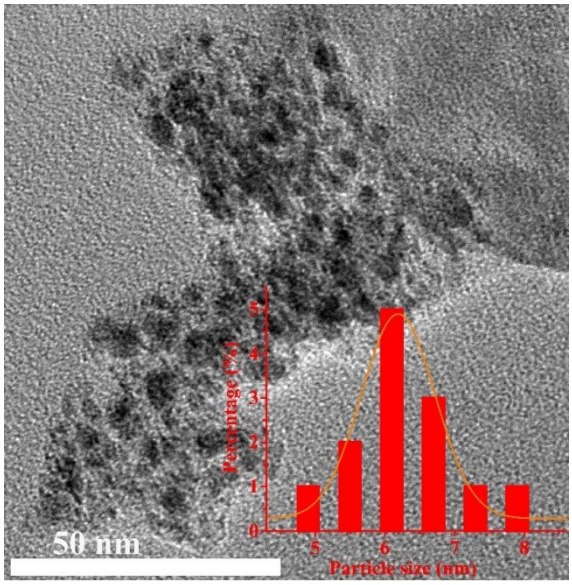

Fig. S13 TEM image of Ru/Mo_2C (Ru wt. % = 4.50 %). Inset (b): Particle size distributions of Ru/Mo_2C.

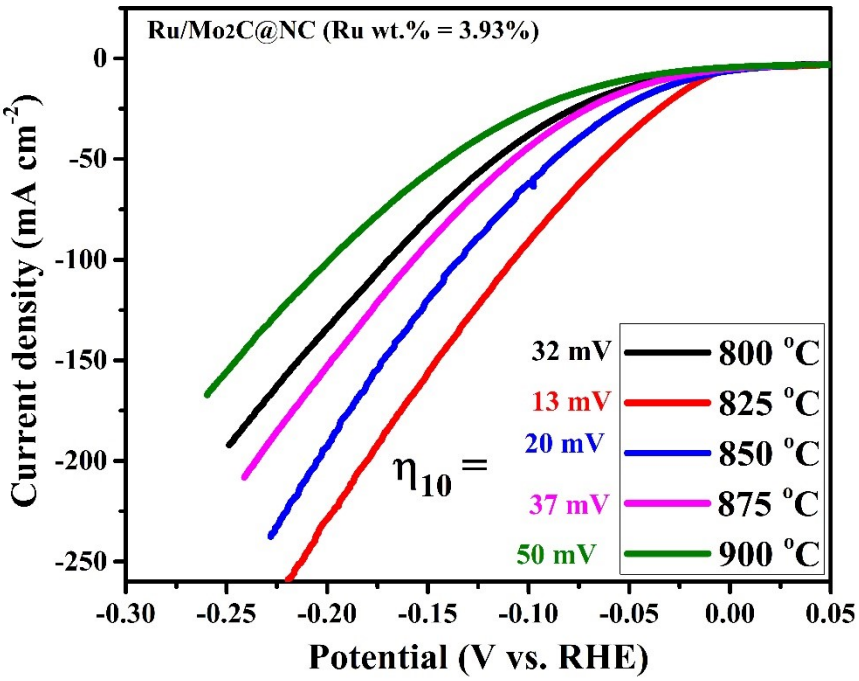

Fig. S14 (a) LSV curves of Ru/Mo_2C@NC (Ru wt. % = 3.93 %) catalysts synthesized at different temperatures in 1 M KOH.

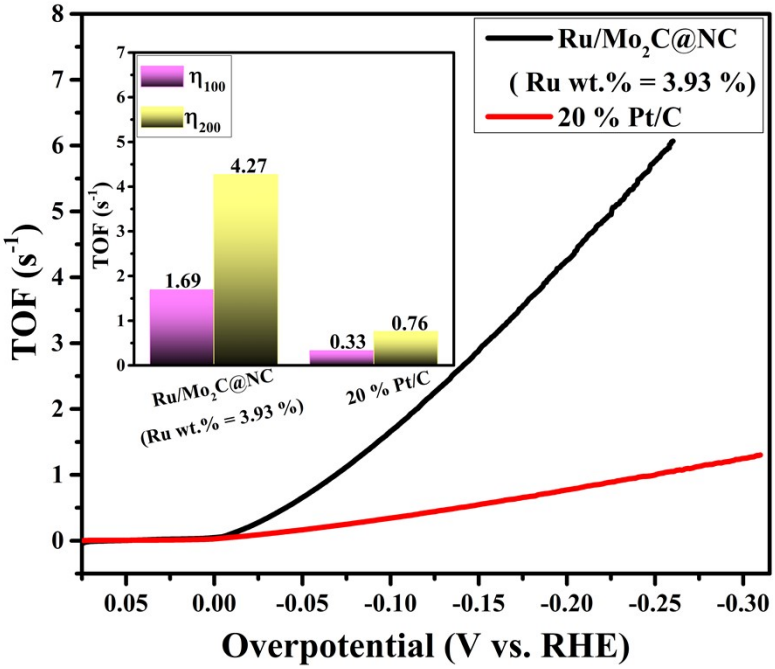

Fig. S15 TOF curves of the Ru/Mo_2C@NC (Ru wt. % = 3.93 %) and 20 % Pt/C catalysts in 1 M KOH; inset: a comparison of the TOF values of catalysts at the different overpotentials (100 mV and 200 mV).

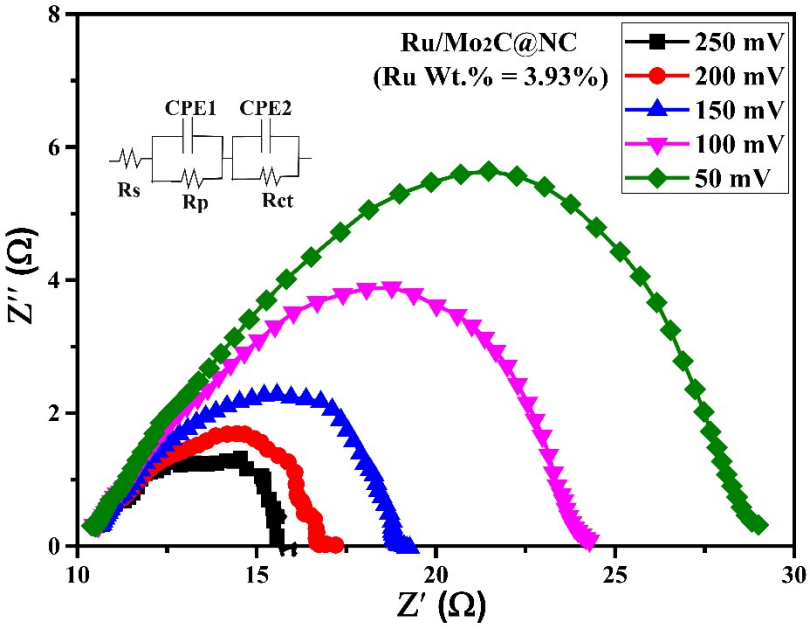

Fig. S16 Electrochemical impedance spectra (EIS) of Ru/Mo_2C@NC (Ru wt. % = 3.93 %) measured with different overpotentials from 50 to 250 mV in 1 M KOH; inset: the model equivalent circuit involving two-time-constant which used for data fitting of EIS spectra.

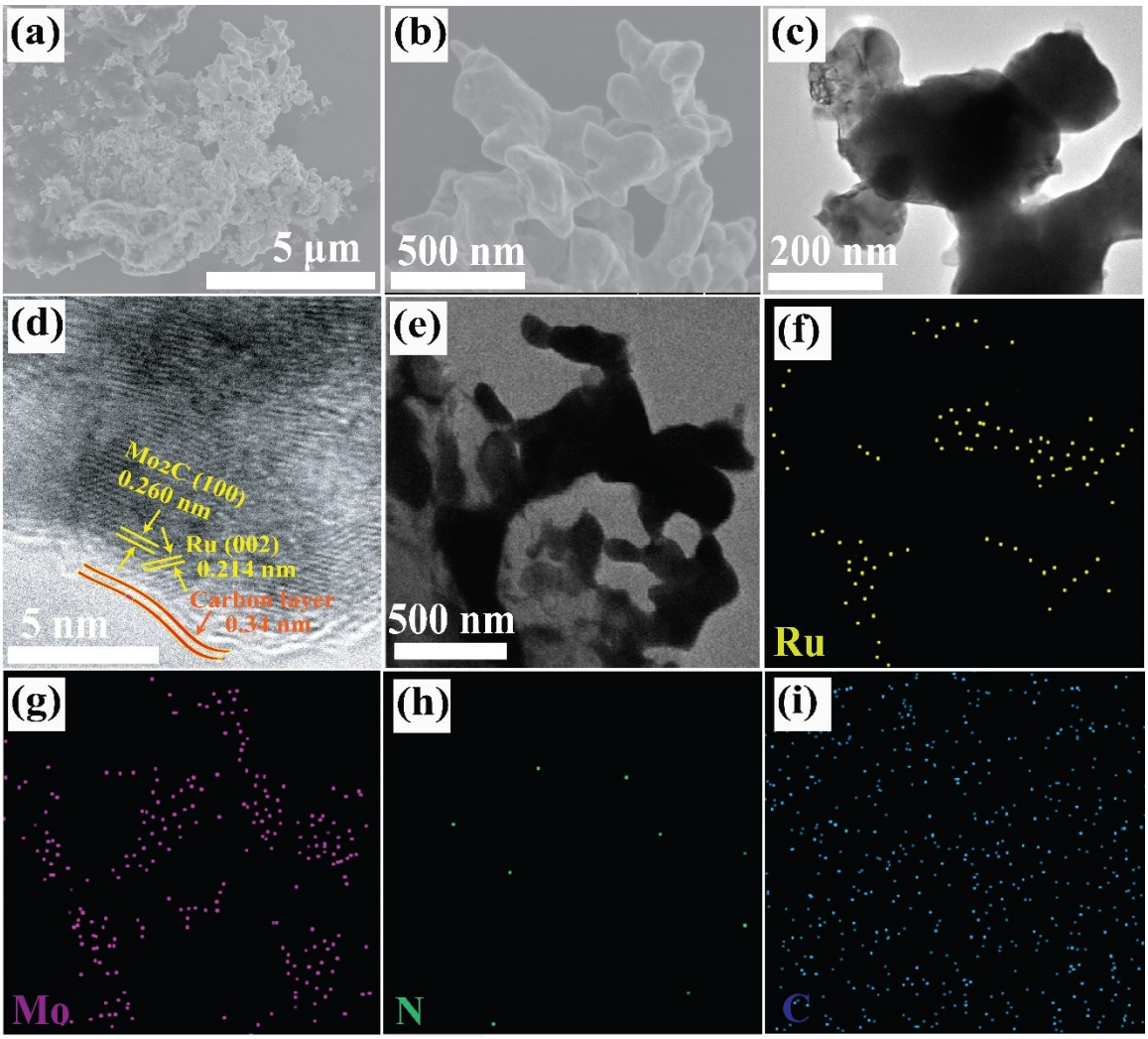

Fig. S17 (a-b) SEM, (c) TEM, and (d) HRTEM images of Ru/Mo_2C@XC-72. (e-i) TEM-EDS elemental mappings of Ru/Mo_2C@XC-72.

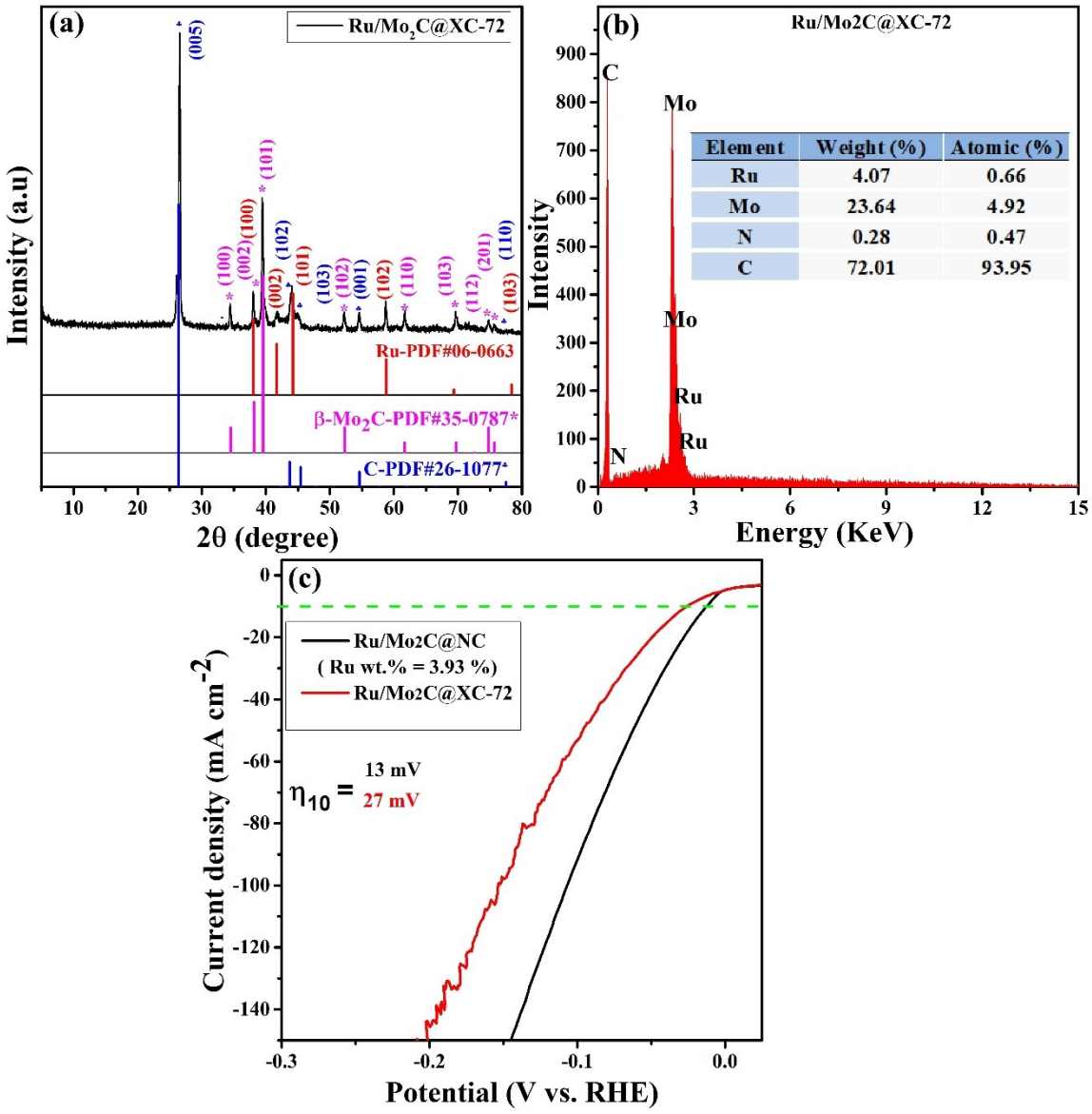

Fig. S18 (a) XRD pattern, (b) EDX spectrum of Ru/Mo_2C@XC-72. (c) Comparison HER LSV curves of Ru/Mo_2C@NC (Ru wt. % = 3.93 %) with Ru/Mo_2C@XC-72 in 1 M KOH.

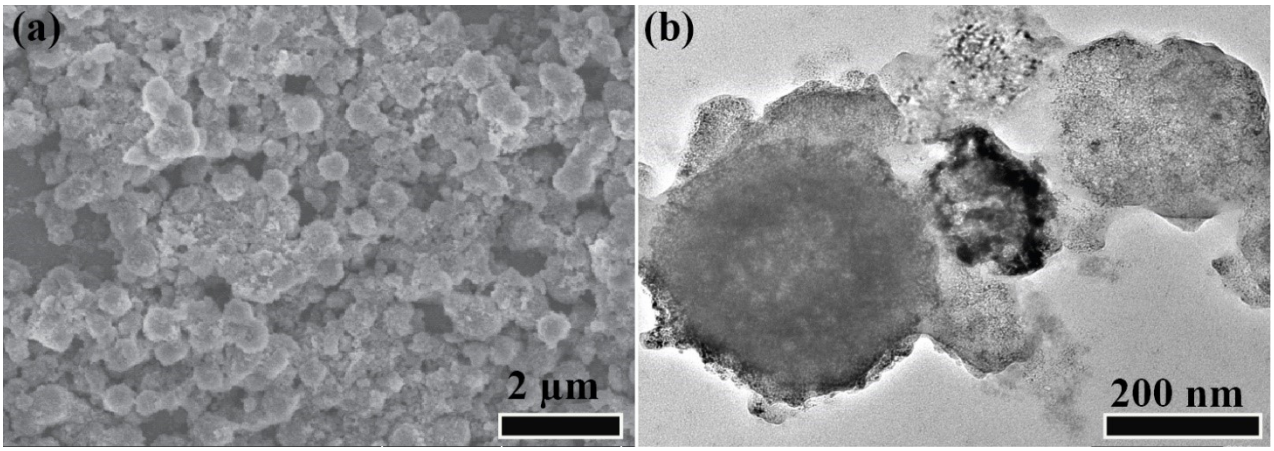

Fig. S19 (a) SEM and (b) TEM images of Ru/Mo_2C@NC (Ru wt. % = 3.93 %) after electrochemical stability test in 1 M KOH.

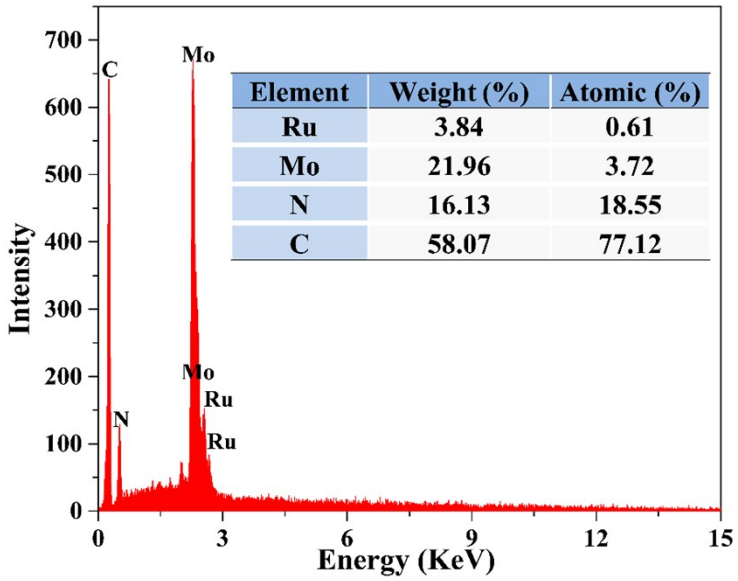

Element	Weight (%)	Atomic (%)
Ru	3.84	0.61
Mo	21.96	3.72
N	16.13	18.55
C	58.07	77.12

Fig. S20 The EDX spectrum of Ru/Mo_2C@NC (Ru wt. % = 3.93 %) after electrochemical stability test in 1 M KOH.

As demonstrated in the above images, the morphology of the Ru/Mo_2C@NC (Ru wt. % = 3.93 %) catalyst shows a slight change after the electrochemical stability test

because some hollow spheres are destroyed as a result of the magnetic stringing during the long-term stability test for 72 h.

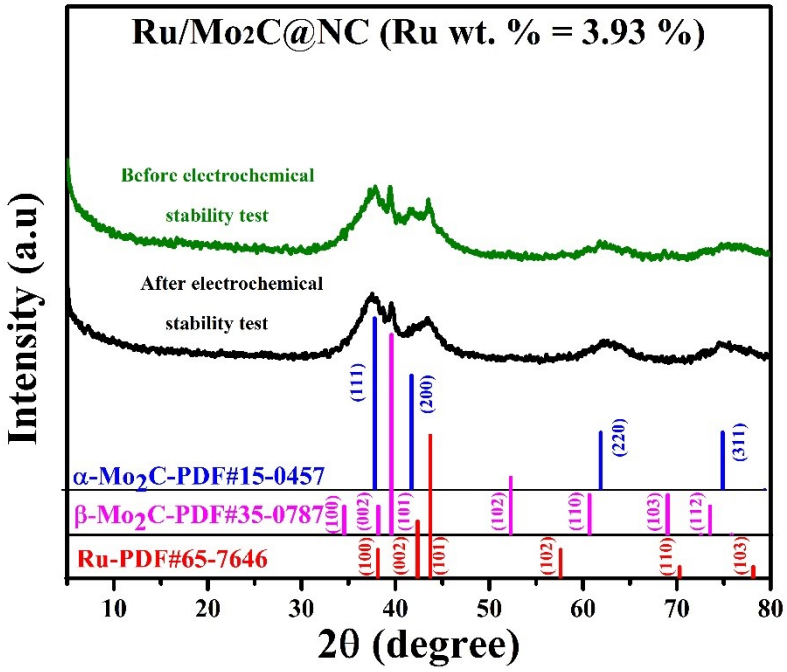

Fig. S21 XRD patterns of Ru/Mo_2C@NC (Ru wt. % = 3.93 %) catalyst before and after electrochemical stability test in 1 M KOH.

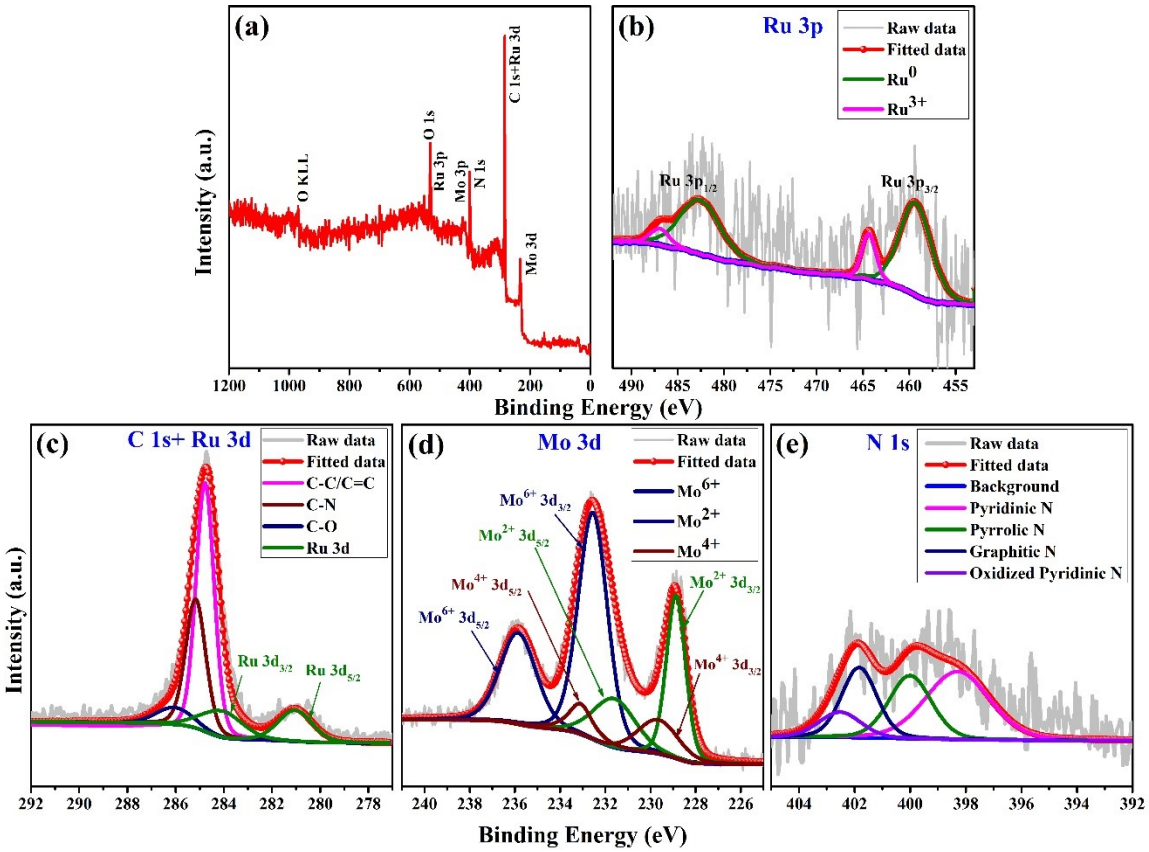

Fig. S22 XPS spectra of Ru/Mo_2C@NC (Ru wt. % = 3.93 %) catalyst after electrochemical stability test in 1 M KOH. (a) The full XPS survey spectrum of Ru/Mo_2C@NC (Ru wt. % = 3.93 %) catalyst. (b–e) High-resolution XPS spectra of Ru/Mo_2C@NC (Ru wt. % = 3.93 %): (b) Ru 3p, (c) C 1s + Ru 3d, (d) Mo 3d, and (e) N 1s.

From the EDX, XRD, and XPS figures, it can be seen that the Ru/Mo_2C@NC (Ru wt. % = 3.93 %) catalyst still retains the initial composition elements as before the electrochemical stability test.

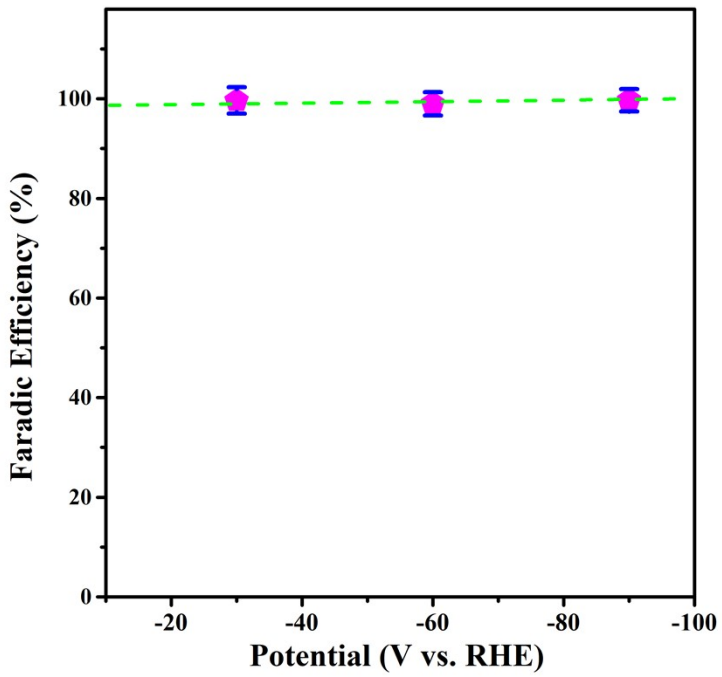

Fig. S23 Faradaic efficiency of H_2 achieved by Ru/Mo_2C@NC (Ru wt. % = 3.93 %) towards the HER at various overpotentials of 30, 60, and 90 mV in 0.5 M H_2SO_4.

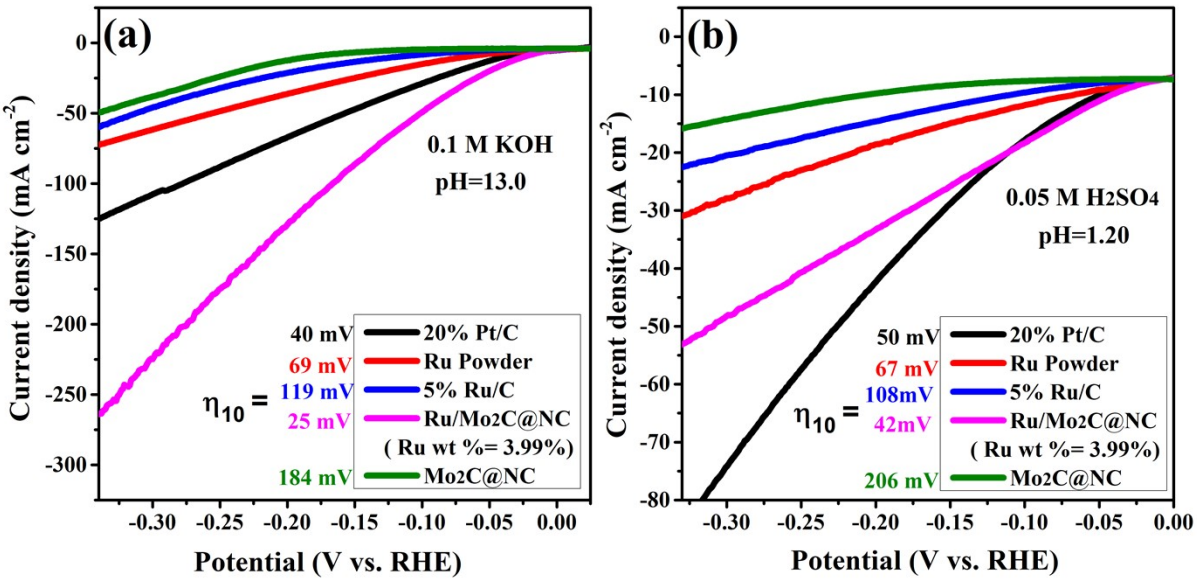

Fig. S24 LSV curves of different catalysts Ru/Mo_2C@NC (Ru wt. % = 3.93 %), 20 % Pt/C, 5 % Ru/C, Ru powder, and Mo_2C@NC catalysts in the universal-pH (a) 0.1 M KOH, (b) 0.05 M H_2SO_4.

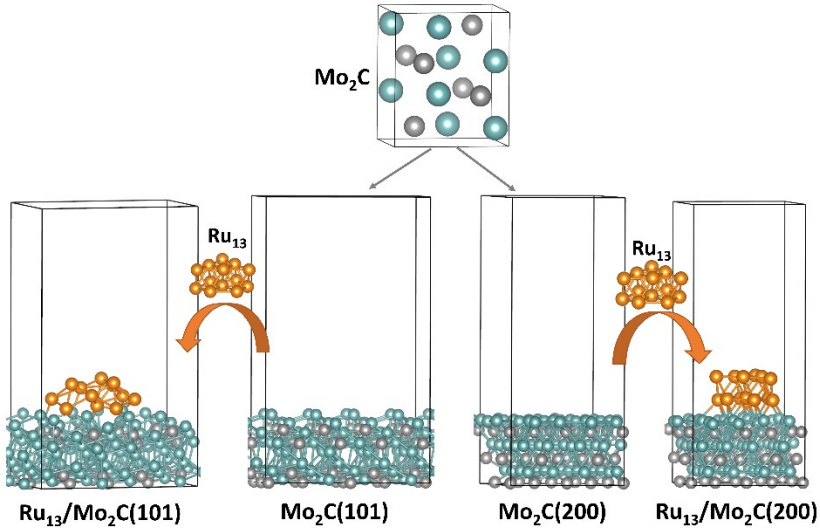

Fig. S25 Bulk crystallographic structure of orthorhombic Mo_2C and two slab models $Mo_2C(101)$ and $Mo_2C(200)$ generated from the bulk. Green, grey, and orange atoms are Mo, C, and Ru, respectively.

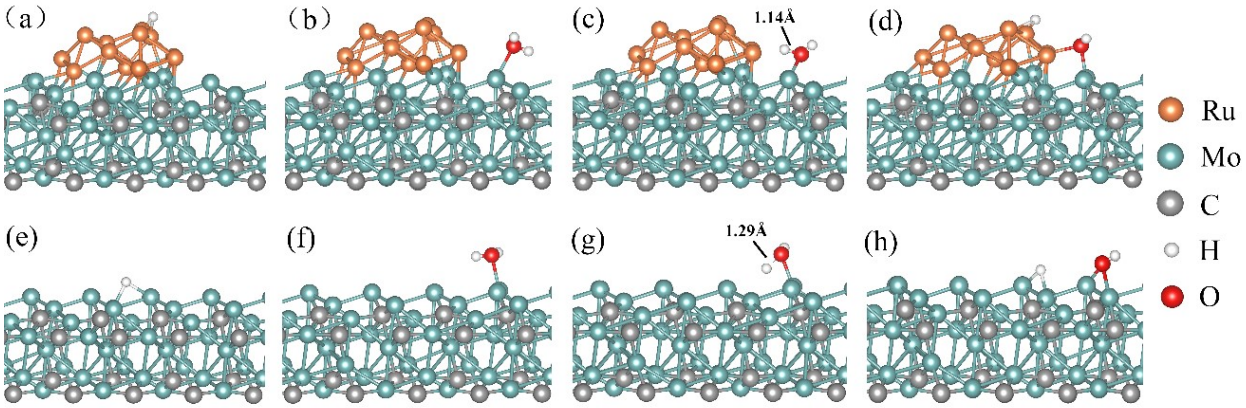

Fig. S26 Configurations of H* adsorption on Ru_{13}/Mo_2C (a) and Mo_2C (e); Initial state, transition state and final state of water splitting on Ru_{13}/Mo_2C (b,c,d) and Mo_2C (f,g,h).

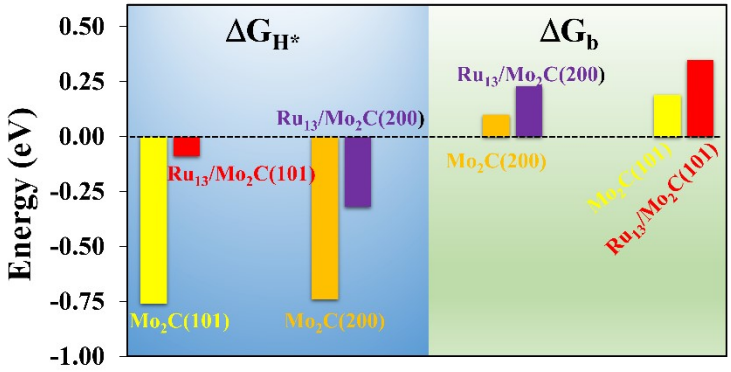

Fig. S27 The comparison of H adsorption (left) and water dissociation barrier (right) on pure $Mo_2C(101)$, $Mo_2C(_200)$, and composite $Ru_{13}/Mo_2C(101)$, $Ru_{13}/Mo_2C(101)$ surfaces.

4. Supporting Tables

Table S1. The EDX and ICP results of Ru/Mo_2C@NC catalysts with different Ru mass loading.

Catalyst **Ru content (wt. %)** **Characterization methods**	**EDAX** **(wt. %)**	ICP **(wt. %)**
Mo_2C@NC	0.07	0
Ru/ Mo_2C@NC (Ru wt. % = 2.56 %)	2.41	2.56
Ru/ Mo_2C@NC (Ru wt. % = 3.07 %)	2.96	3.07
Ru/ Mo_2C@NC (Ru wt. % = 3.25 %)	3.38	3.45
Ru/ Mo_2C@NC **(Ru wt. % = 3.93 %)**	**4.02**	**3.93**
Ru/ Mo_2C@NC (Ru wt. % = 4.50 %)	4.62	4.50

Table S2. Comparison of the HER performance of Ru/Mo_2C@NC (Ru wt. % = 3.93 %) with other Ru-based electrocatalysts towards HER in pH-universal.

Catalyst	Electrolyte	η_{10} (mV)	Tafel slope (mV dec^{-1})	Reference
Ru/Mo_2C@NC (Ru wt. % = 3.93 %)	**1 M KOH**	**13**	**33.24**	**This work**
	0.5 M H_2SO_4	**21**	**43.36**	
	1 M PBS	**41**	**58.87**	
RuNi/CQDs	1 M KOH	13	40	S[13]
	0.5 M H_2SO_4	58	55	
	1 M PBS	18	76	
Ru@CN-0.16	1 M KOH	32	53	S[10]
	0.5 M H_2SO_4	126	-	
	1 M PBS	100	-	
RuP_2@NPC	1 M KOH	52	69	S[14]
	0.5 M H_2SO_4	38	38	
	1 M PBS	57	87	
Ru-NiFeP/NF	1 M KOH	56	68	S[15]
	0.5 M H_2SO_4	29	56	
	1 M PBS	105	83	
Ru@SC-CDs	1 M KOH	29	57	S[16]
	0.5 M H_2SO_4	59	52	
	1 M PBS	66	158	
NiRu@N-C	1 M KOH	32	64	S[17]
	0.5 M H_2SO_4	50	36	
	1 M PBS	482	-	
Ru SAs–Ni_2P	1 M KOH	57	75	S[18]
	0.5 M H_2SO_4	125	71	
	1 M PBS	260	-	

Table S3. The electrochemical parameters of Ru/Mo_2C@NC (Ru wt. % = 3.93 %) and other control electrocatalysts for HER in 1 M KOH.

Catalyst	η_{10} (mV)	Mass Activity[a] ($mA\ mg^{-1}$)	Tafel Slope ($mV\ dec^{-1}$)	j_0[b] ($mA\ cm^{-2}$)
Ru/Mo_2C@NC (Ru wt. % = 3.93 %)	**13**	**755.58**	**33.24**	**7.54**
20% Pt/C	19	107.74	32.55	5.21
5% Ru/C	67	48.66	58.62	3.73
Ru Powder	43	9.36	65.71	2.27

[a] The current densities at an overpotential of 50 mV. [b] Exchange current densities (j_0) are obtained from Tafel curves by using the extrapolation method.

Table S4. The electrochemical parameters of Ru/Mo_2C@NC with different Ru content (wt. %) for HER in 1 M KOH.

Catalyst	η_{10} (mV)	Mass Activity[a] ($mA\ mg^{-1}$)	Tafel Slope ($mV\ dec^{-1}$)	j_0[b] ($mA\ cm^{-2}$)
Ru/Mo_2C@NC (Ru wt. % = 2.56 %)	63	475.52	66.43	2.53
Ru/Mo_2C@NC (Ru wt. % = 3.07 %)	34	446.36	54.54	3.19
Ru/Mo_2C@NC (Ru wt. % = 3.45 %)	27	401.47	46.19	3.98
Ru/Mo_2C@NC (Ru wt. % = 3.93 %)	**13**	**755.58**	**33.24**	**7.54**
Ru/Mo_2C@NC (Ru wt. % = 4.50 %)	20	646.18	39.51	5.27

[a] The current densities at an overpotential of 50 mV. [b] Exchange current densities (j_0) are obtained from Tafel curves by using the extrapolation method.

Table S5. The resistances (Rct) and a series resistance (Rs) values of the different catalysts at overpotential (mV *vs.* RHE) of 200 mV in 1 M KOH.

Catalyst	R_{ct} (Ω)	R_s (Ω)
Ru/Mo_2C@NC (Ru wt. % = 3.93 %)	**3.77**	**5.51**
20 % Pt/C	5.20	6.67
5 % Ru/C	7.53	6.76
Ru Powder	9.11	6.25
Mo_2C@NC	53.02	6.26
Mo_2C@C	60.84	6.17

Table S6. The resistances (R_{ct}) and series resistance (Rs) values of Ru/Mo_2C@NC (Ru wt. % = 3.93 %) with overpotentials from 50 to 250 mV in 1 M KOH.

Overpotential (mV vs. RHE)	**Ru/Mo_2C@NC (Ru wt. % = 3.93 %)**	
	R_{ct} (Ω)	R_s (Ω)
50	9.76	5.61
100	6.45	5.77
150	4.59	5.48
200	3.77	5.35
250	2.21	5.57

Table S7. The electrochemical parameters of Ru/Mo_2C@NC (Ru wt. % = 3.93 %) and other control electrocatalysts for HER in 0.5 M H_2SO_4.

Catalyst	η_{10} (mV)	Mass Activity[a] ($mA\ mg^{-1}$)	Tafel Slope ($mV\ dec^{-1}$)	j_0[b] ($mA\ cm^{-2}$)
Ru/Mo_2C@NC (Ru wt. % = 3.93 %)	**21**	**526.09**	**43.36**	**6.75**
20% Pt/C	26	125.51	31.11	4.51
5% Ru/C	211	20.60	75.52	3.88
Ru Powder	126	2.27	53.78	2.69

[a] The current densities at an overpotential of 50 mV. [b] Exchange current densities (j_0) are obtained from l curves by using the extrapolation method.

Table S8. The electrochemical parameters of Ru/Mo_2C@NC (Ru wt. % = 3.93 %) and other control electrocatalysts for HER in 1 M PBS.

Catalyst	η_{10} (mV)	Mass Activity[a] ($mA\ mg^{-1}$)	Tafel Slope ($mV\ dec^{-1}$)	j_0[b] ($mA\ cm^{-2}$)
Ru/Mo_2C@NC (Ru wt. % = 3.93 %)	**41**	**230.36**	**58.87**	**4.19**
20% Pt/C	59	60.44	63.62	2.60
5% Ru/C	112	59.06	108.27	2.42
Ru Powder	70	36.18	83.76	2.46

[a] The current densities at an overpotential of 50 mV. [b] Exchange current densities (j_0) are obtained from l curves by using the extrapolation method.

Table S9. The resistances (R_{ct}) and series resistance (Rs) values of Ru/Mo_2C@NC (Ru wt. % = 3.93 %) with overpotentials from 50 to 200 mV in 0.5 M H_2SO_4.

Overpotential (mV vs. RHE)	**Ru/Mo_2C@NC (Ru wt. % = 3.93 %)**	
	R_{ct} (Ω)	R_s (Ω)
50	15.06	6.62
100	11.88	6.25
150	7.46	6.68
200	3.70	6.57

Table S10. The resistances (R_{ct}) and series resistance (Rs) values of Ru/Mo_2C@NC (Ru wt. % = 3.93 %) with overpotentials from 50 to 200 mV in 1 M PBS.

Overpotential (mV vs. RHE)	**Ru/Mo_2C@NC (Ru wt. % = 3.93 %)**	
	R_{ct} (Ω)	R_s (Ω)
50	484.1	7.83
100	37.53	7.49
150	14.65	7.23
200	10.49	7.01

Additional references

S1. C. Coutanceau, M. Croissant, T. Napporn and C. Lamy, *Electrochim. Acta*, 2000, **46**, 579-588.

S 2. L. An, L. Huang, P. Zhou, J. Yin, H. Liu and P. Xi, *Adv. Funct. Mater.*, 2015, **25**, 6814-6822.

S 3. M. R. Gao, J. X. Liang, Y. R. Zheng, Y. F. Xu, J. Jiang, Q. Gao, J. Li and S. H. Yu, *Nat. Commun.*, 2015, **6**, 1-7.

S 4. M. R. Khan, T. W. Chuan, A. Yousuf, M. Chowdhury and C. K. Cheng, Catal. Sci. Technol., 2015, **5**, 2522-2531.

S 5. B. Q. Qiu, C. X. Li, X. Q. Shen, W. L. Wang, H. Ren, Y. Li and J. Tang, Appl. Catal. A: Gen., 2020, **592**, 117377.

S 6. Z. Zhuang, Y. Li, Z. Li, F. Lv, Z. Lang, K. Zhao, L. Zhou, L. Moskaleva, S. Guo and L. Mai, *Angew. Chem. Int. Ed.*, 2018, **57**, 496-500.

S 7. B. JO'M and P. Subramanyan, *Electrochim. Acta*, 1971, **16**, 2169-2179.

S 8. Q. Liu and A. Atrens, 2014, *Corros. Sci.*, **87**, 239-258.

S 9. B. Conway, L. Bai and M. Sattar, Int. J. Hydrog. Energy, 1987, **12**, 607-621.

S 10. J. Wang, Z. Wei, S. Mao, H. Li and Y. Wang, *Energy Environ. Sci.*, 2018, **11**, 800-806.

S 11. J. Tian, Q. Liu, A. M. Asiri and X. Sun, *J. Am. Chem. Soc.*, 2014, **136**, 7587-7590.

S 12. Y. Y. Ma, Z. L. Lang, L.-K. Yan, Y. H. Wang, H. Q. Tan, K. Feng, Y. J. Xia, J. Zhong, Y. Liu and Z. H. Kang, *Energy Environ. Sci.*, 2018, **11**, 2114-2123.

S 13. Y. Liu, X. Li, Q. Zhang, W. Li, Y. Xie, H. Liu, L. Shang, Z. Liu, Z. Chen and L. Gu, *Angew. Chem. Int. Ed.*, 2020, **59**, 1718-1726.

S 14. Z. Pu, I. S. Amiinu, Z. Kou, W. Li and S. Mu, *Angew. Chem. Int. Ed.*, 2017, **56**, 11559-11564.

S 15. Y. Lin, M. Zhang, L. Zhao, L. Wang, D. Cao and Y. Gong, *Appl. Surf. Sci.*, 2021, **536**, 147952.

S 16. Y. Liu, Y. Yang, Z. Peng, Z. Liu, Z. Chen, L. Shang, S. Lu and T. Zhang, *Nano Energy*, 2019, **65**, 104023.

S 17. Y. Xu, S. Yin, C. Li, K. Deng, H. Xue, X. Li, H. Wang and L. Wang, *J. Mater. Chem. A*, 2018, **6**, 1376-1381.

S 18. K. Wu, K. Sun, S. Liu, W. C. Cheong, Z. Chen, C. Zhang, Y. Pan, Y. Cheng, Z. Zhuang and X. Wei, *Nano Energy*, 2021, **80**, 105467.